


 Cite this: *RSC Adv.*, 2023, **13**, 13252

# Highly thermal conductive shape-stabilized composite phase change materials based on boron nitride and expanded graphite for solar thermal applications

 Dongfang Huang,<sup>ab</sup> Guixiang Ma,<sup>id</sup>\*<sup>c</sup> Zhixiao Yu,<sup>c</sup> Peng Lv,<sup>b</sup> Quanbao Zhou,<sup>d</sup> Quanyu Liu,<sup>b</sup> Cheng Peng,<sup>b</sup> Fan Xiong<sup>b</sup> and Yan Huang<sup>b</sup>

Phase change heat storage technology is a good way to solve the problem that the temperature of solar hot water outlet is affected by the time domain. A stearic acid (SA)–benzamide (BA) eutectic mixture is a potential phase change material (PCM), but it still has the disadvantages of low thermal conductivity and liquid leakage. In this work, a new high thermal conductive shape-stabilized composite PCM was prepared by adding boron nitride (BN) and expanded graphite (EG) to a melted SA–BA eutectic mixture using an ultrasonic and melt adsorption method, and its phase change temperature, latent heat, crystal structure, morphology, thermal conductivity, chemical stability, thermal stability, cycle stability and leakage characteristics were characterized. The results indicates that the addition of BN and EG significantly improved the thermal conductivity of the SA–BA eutectic mixture, and they efficiently adsorbed the melted SA–BA eutectic mixture. Besides, when the mass fractions of BN and EG are 15 wt% and 20 wt%, respectively, the 15BN20EG composite has almost no liquid phase leakage. When the melting enthalpy and temperature of 15BN20EG are 132.35 J g<sup>-1</sup> and 65.21 °C, respectively, the thermal conductivity of the 15BN20EG is 6.990 W m<sup>-1</sup> K<sup>-1</sup>, which is 20.601 times that of the SA–BA eutectic mixture. Moreover, 15BN20EG shows good thermal stability after 100 cycles and good chemical stability below 100 °C. Therefore, the 15BN20EG composite is considered as a potential candidate for solar thermal applications.

Received 21st February 2023

Accepted 22nd April 2023

DOI: 10.1039/d3ra01166f

[rsc.li/rsc-advances](http://rsc.li/rsc-advances)

## 1. Introduction

The increasingly serious environmental pollution and fossil energy crisis have attracted much attention. Fatty acid organic phase change latent heat materials are considered to be promising PCMs due to their high latent heat capacity, suitable solid–liquid transition temperature, low supercooling degree, self-nucleation, good chemical stability, good thermal stability, non-toxicity, being non-corrosive, low cost and small volume change during phase change. In recent years, it has been extensively studied in the field of solar energy storage units, air conditioning heat transfer systems, thermal comfort thermostat buildings and so on.<sup>1–3</sup> However, the development of fatty acid organic phase change materials (PCMs) is limited by factors

such as low thermal conductivity and easy liquid leakage during solid–liquid phase transformation. The selection of nanofillers can effectively improve the thermal conductivity, such as, silicon dioxide,<sup>4,5</sup> BN,<sup>6</sup> aluminum oxide,<sup>7</sup> aluminum nitride,<sup>8</sup> carbon nanotube,<sup>9</sup> and titanium dioxide.<sup>10</sup>

Hexagonal boron nitride (BN) as one of the high thermal conductivity fillers, it is a typical graphite-like material with a crystal structure similar to graphite.<sup>11</sup> It is widely used because of its good thermal stability, good thermal conductivity, and electrical insulation, low dielectric constant and low coefficient of thermal expansion.<sup>12–17</sup> Xie *et al.*<sup>18</sup> prepared SA/BN composite PCMs by vacuum impregnation. The result indicates that the thermal conductivity of the composite (0.453 W m<sup>-1</sup> K<sup>-1</sup>) is enhanced by 73.36% compared to pure SA (0.261 W m<sup>-1</sup> K<sup>-1</sup>), showing a good heat transfer efficiency. Ao<sup>19</sup> using melting in the blending method prepared SA/BN composite PCMs, the thermal conductivity of SA/BN composite PCMs is 2.82 times higher compared to pure SA. Su *et al.*<sup>20</sup> employed BN as the thermally conductive fillers and SA-*n*-octadecane eutectic mixtures as PCMs to prepare SA-*n*-octadecane/BN composites, the thermal conductivity of the SA-*n*-octadecane eutectic increases from 0.2982 W m<sup>-1</sup> K<sup>-1</sup> to 0.3220 W m<sup>-1</sup> K<sup>-1</sup> at 20 °C

<sup>a</sup>Engineering Research Center of Nuclear Technology Application, East China University of Technology, Ministry of Education, Nanchang, 330013, China

<sup>b</sup>School of Water Resources and Environmental Engineering, East China University of Technology, 330013, China

<sup>c</sup>Teachers' College, East China University of Technology, Nanchang 330013, P. R. China. E-mail: guixiangm@qq.com

<sup>d</sup>School of Chemistry and Material Science, East China University of Technology, Nanchang 330013, P. R. China



Table 1 Chemical reagents used in this study

Chemical name	Source	Mass fraction purity <sup>a</sup>	Purification method
SA	Sinopharm Chemical Reagent Co., Ltd	0.98 (AR)	None
BA	Aladdin Industrial Corporation (Shanghai, China)	0.99 (AR)	None
BN	Aladdin Industrial Corporation (Shanghai, China)	99.8%	None

<sup>a</sup> According to the supplier.

and from  $0.1512 \text{ W m}^{-1} \text{ K}^{-1}$  to  $0.1764 \text{ W m}^{-1} \text{ K}^{-1}$  at  $40 \text{ }^\circ\text{C}$ , respectively, due to introduction of the 10 wt% BN. Overall the literature shows a consensus around the fact that the addition of BN brings improvement in the thermal conductivity of fatty acid PCMs. However, the increase of the thermal conductivity of composite PCMs by BN is limited. Moreover, after several thermal cycles, the BN are easy to agglomerate and precipitate, which worsens the thermal properties of PCMs.

To further improve thermal conductivity and enhance the thermal physical properties of organic PCMs, the use of inorganic matrices has been proposed. By using inorganic matrices with a relatively big surface area and micro-structure as the supporting material, the PCM is absorbed into the micro-pores *via* capillary forces to form a shape-stabilized composite material. EG, as one of inorganic matrices because of its rich network structure, large specific surface area, good adsorption properties and a large number of heat conduction chains, is widely used for thermal energy storage.<sup>21–23</sup> Isarn *et al.*<sup>24</sup> added EG and BN to epoxy, which improves the thermal conductivity of epoxy. Ao *et al.*<sup>25</sup> prepared SA/BN/EG composite PCMs by adding boron BN and EG to melted SA, when the mass fraction of BN and EG was 12 wt%, the thermal conductivity of the composite was  $6.349 \text{ W m}^{-1} \text{ K}^{-1}$ , which was 18.619 times that of SA. Moreover, the composite showed good stability for 50 cycles of heating and cooling, and the SA/BN/EG-12 hardly decomposes below  $200 \text{ }^\circ\text{C}$ , which implies that the working performance of the composite PCMs has good thermal stability within the temperature range of  $100 \text{ }^\circ\text{C}$ .

Therefore, the purpose of this study is to develop a PCMs with latent heat that does not decrease significantly and maximum thermal stability and thermal conductivity. The SA-BA/BN/EG composite PCMs was prepared by adding BN and EG to melted SA-BA eutectic mixture using ultrasonic and melting impregnation method. Then, the phase change temperature, latent heat, crystal structure, morphology, thermal stability, cycle stability, thermal conductivity and liquid leakage of composite PCMs were analyzed and studied to determine their application potential in the thermal energy storage system.

## 2. Experimental

### 2.1. Materials

Stearic acid (SA, purity  $\geq 98\%$ , analytical reagent (A. R.)) was purchased from Sinopharm Chemical Reagent Co., Ltd. Benzamide (BA,  $\geq 99\%$ , A. R.) were obtained from Aladdin Industrial Corporation, and they were used as received. Expandable graphite (grade XF057,  $300 \mu\text{m}$ , expandable coefficient:  $350 \text{ mL g}^{-1}$ ) has

a carbon content of 98%, a density of  $2.26 \text{ g cm}^{-3}$  was received from Nanjing XFNANO Materials Tech Co., Ltd. And expandable graphite was dried in an oven for 24 h at  $100 \text{ }^\circ\text{C}$  before used. Hexagonal boron nitride (BN;  $100 \text{ nm}$ , thermal conductivity:  $33 \text{ W m}^{-1} \text{ K}^{-1}$ ) was bought from Shanghai Aladdin Biochemical Co., Ltd (Shanghai, China). Their purity was attained from manufacture, and these data were listed in Table 1.

### 2.2. Preparation of SA-BA/BN/EG composites

In this experiment, the mass ratio of SA-BA was determined to be 88.0% SA and 12.0% BA by the theoretical calculation and in reference to a previous research.<sup>23</sup> A series of SA-BA/BN/EG composites were prepared with SA-BA eutectic mixture as the PCMs, EG as the support material and BN as the heat conduction enhancer. The preparation process is as follows: first, weigh a certain amount of SA and BA with the determined mass ratio in a round bottom flask according to the proportion, put them in a collector constant temperature magnetic heating stirrer, heat and stir them for 20 min at  $120 \text{ }^\circ\text{C}$ , after the materials are completely melted into liquid and mixed evenly, put the round bottom flask in an ultrasonic cleaner whose temperature is maintained within the range of  $70\text{--}100 \text{ }^\circ\text{C}$ , and then add BN powder with a certain mass ratio to the eutectic mixture, and ultrasonic for 10 min. Second, slowly add EG with a certain mass ratio into the flask in batches with a triangular funnel, and stir with a glass rod to mix the materials of each component evenly, and then ultrasonic for 3 h. Finally, stir it evenly and cool it at room temperature to prepare SA-BA/BN/EG composite. The conceptual design of composite material is shown in Fig. 1. The names of the composite at different mass ratio are shown in Table 2.

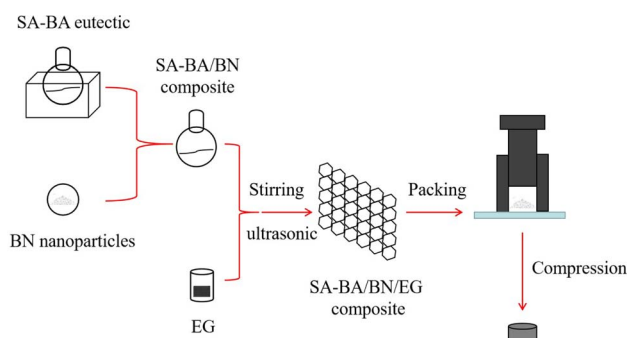


Fig. 1 Schematic diagram of prepared SA-BA/BN/EG composite.



Table 2 Mass fraction of composite

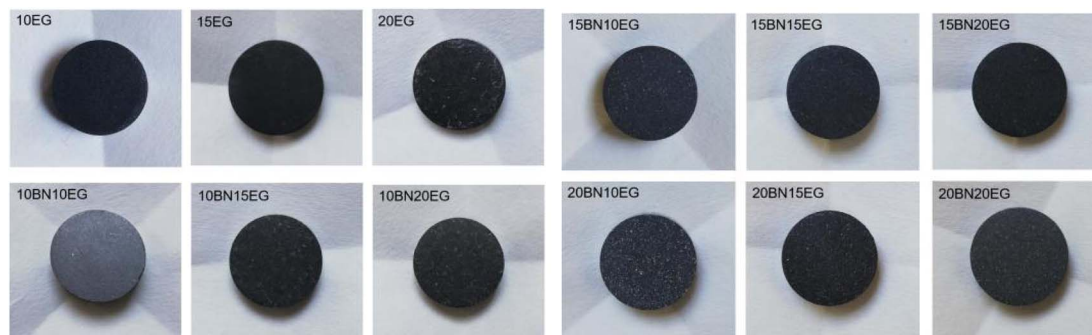
Sample	SA-BA (wt%)	BN (wt%)	EG (wt%)
10EG	90	0	10
15EG	85	0	15
20EG	80	0	20
10BN	90	10	0
15BN	85	15	0
20BN	80	20	0
10BN10EG	80	10	10
10BN15EG	75	10	15
10BN20EG	70	10	20
15BN10EG	75	15	10
15BN15EG	70	15	15
15BN20EG	65	15	20
20BN10EG	70	20	10
20BN15EG	65	20	15
20BN20EG	60	20	20

### 2.3. Characterization

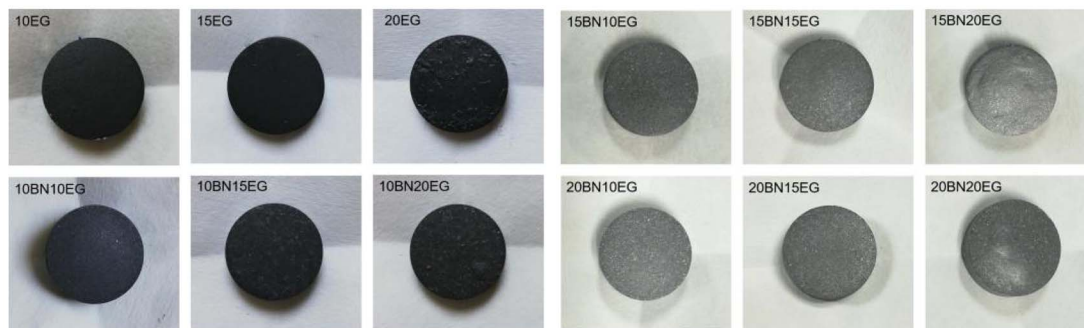
The chemical compatibility of sample was evaluated by Fourier transform infrared spectroscopy (FTIR, Nicolet Nexus 670). The crystal structure and chemical compatibility of sample were studied by PANalytical X'PRO Pert diffractometer. The morphology and structure of the samples were observed by using a JSM-5601LV high vacuum tungsten filament emission scanning electron microscope (SEM) from JEOL at 2 kV. The

phase change behavior of sample were measured by a differential scanning calorimeter (DSC, Mettler Toledo DSC 2, Switzerland) at a rate of  $10\text{ }^{\circ}\text{C min}^{-1}$  under a nitrogen atmosphere. The DSC was calibrated by using the standard samples indium. The uncertainties of the DSC for the phase transition temperature and latent heat are  $\pm 1\text{ }^{\circ}\text{C}$  and  $\pm 5\%$ , respectively. The onset temperature of the DSC measurement is considered as phase transition temperature. The thermal conductivity of the sample at room temperature was tested by transient plane heat source method using a hot disk thermal constant analyzer (TPS 2500, Hot Disk AB Company, Sweden). The thermal conductivity accuracy is 3%. Before the measurement, the cylindrical samples were pressed with a molding under 15 MPa to obtain discs (diameter of 20 mm). The thermal stability and decomposition properties of the samples was investigated by means of thermo-gravimetry (TG)/differential thermal analysis (DTA) on a thermogravimetric analyzer (NETZSCH, STA 449F3, Germany) under an atmosphere of nitrogen with the heating rate of  $5\text{ }^{\circ}\text{C min}^{-1}$ . The thermal reliability of sample was investigated by accelerated thermal cycle test, and it was carried out by DSC for 100 cycles at rate of  $10\text{ }^{\circ}\text{C min}^{-1}$ .

The liquid leakage of composite was tested by using the filter paper imprint method. The specific steps are as follows: first, weigh a composite PCMs with a mass of about 2 g and press it with a tabletop powder tablet press under a mold diameter of 20 mm and a pressure of 15 MPa to obtain a massive composite. Next, place the prepared samples on the same clean filter paper.



(a) before



(b) after

Fig. 2 Images of SA-BA/BN/EG composite (a) before and (b) after thermal treatment.



Then, it was put into a thermostatic drying oven with a temperature of 100 °C (higher than the melting temperature of the PCMs) and heated at a constant temperature for 3 h to ensure that the SA–BA eutectic mixture was completely molten. After that, take out the sample and put it in the room temperature environment. After the composite was cooled to room temperature, remove it from the filter paper and weigh it. Record the mass loss of the composite before and after heating.

### 3. Results and discussion

#### 3.1. Leakage analysis of the SA–BA/BN/EG composite

The images of the leakage of the SA–BA/BN/EG composite before and after heating for 3 h are shown in Fig. 2. It can be seen from the Fig. 2 that the shape of composite hardly changes before and after heat treatment, which indicates the constructed PCMs a shape stabilized PCMs, that's because BN and EG have similar structures, which thus has a significant effect on enhancing the thermal conductivity and stability of the material.

To study the leakage mass loss more clearly, the mass of the sample before and after the test was weighed. The mass loss ratio of SA–BA/BN/EG composite before and after heat treatment are shown in Fig. 3. It can be seen from Fig. 3 that when the mass fraction of BN is constant, the mass loss ratio of SA–BA/BN/EG composite gradually decreased with the increase of the mass fraction of EG. This may be due to the high porosity of EG, so it has a certain adsorption capacity. When the mass fraction of EG is 20%, as the mass fraction of BN increased from 10% to 20%, the mass loss rates of SA–BA eutectic mixture are 0.066%, 0.067% and 0.066%, respectively. In addition, the mass loss rate of 10 wt% BN is consistent with that of 20 wt% BN. This indicates that when the EG mass fraction is added to 20%, the SA–BA eutectic mixture is encapsulated in the void of EG, and only a small amount of BN is needed to achieve complete encapsulation of SA–BA eutectic mixture. When the EG mass fraction was constant, the mass loss ratio of SA–BA/BN/EG composite is also gradually reduced with the increase of BN mass fraction. It indicates that the addition of BN can also effectively prevent the leakage of SA–BA eutectic mixture. When the mass fractions of EG and BN are 15% and 20%, respectively,

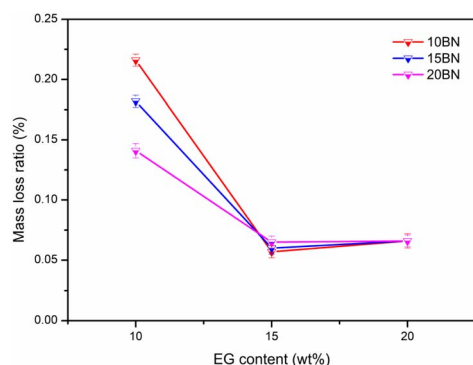


Fig. 3 The mass loss ratio of SA–BA/BN/EG composite after thermal treatment.

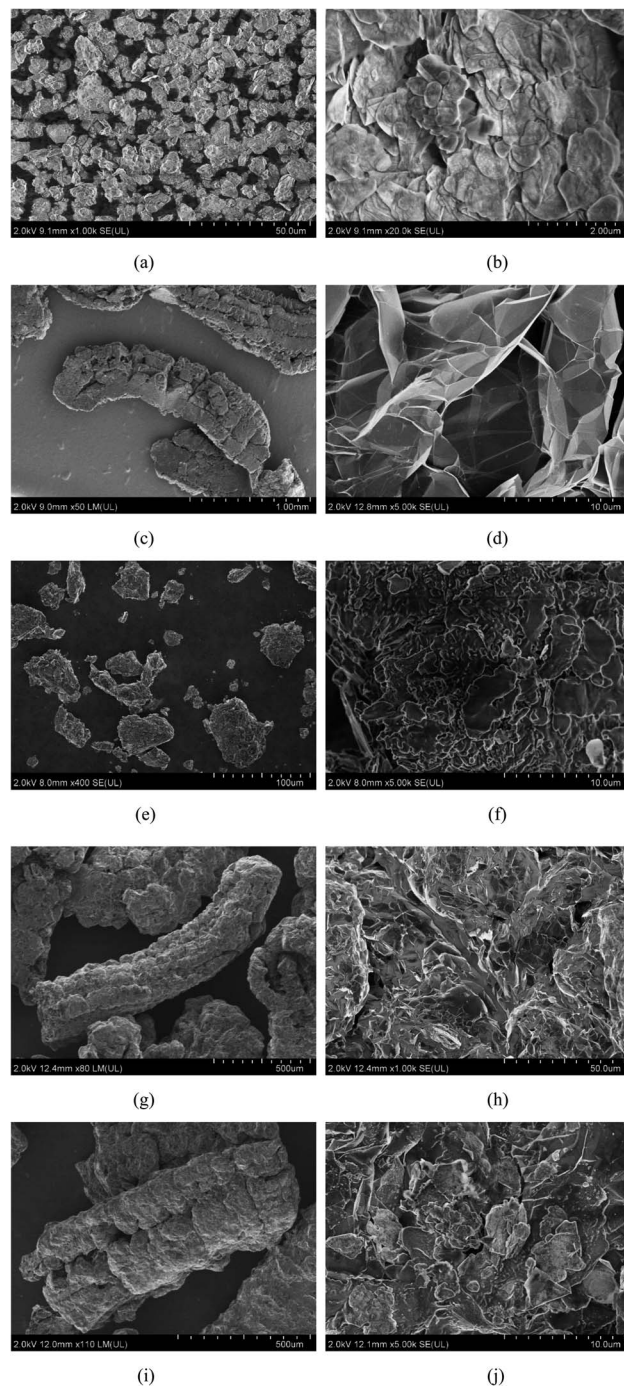


Fig. 4 SEM images of (a and b) BN, (c and d) EG, (e and f) 15BN, (g and h) 20EG, and (i and j) 15BN20EG.

the mass loss rates of 15BN20EG composite are 0.187%, 0.02% and 0.04% lower than those of 10EG, 15EG and 20EG composite, respectively. Which indicates that the porous structure of BN and EG can effectively encapsulate SA–BA eutectic mixture in pores and prevent PCMs from leaking out of pores. In addition, when the mass fraction of EG is lower than 20%, the addition of BN can still lead to the effective encapsulation of SA–BA eutectic mixture. Thus, 15BN20EG has the best performance according to the comprehensive analysis.



### 3.2. Morphology and microstructure of the SA-BA/BN/EG composite

Fig. 4 shows the structure and morphology of SA-BA eutectic mixture, BN, EG, 15BN, 20EG and 15BN20EG composite. It can be seen from Fig. 4(a) and (b) that BN is a lamellar structure and has a relatively large specific surface area at the micro level. As shown in Fig. 4(c) and (d), EG prepared by microwave method shows the worm-like structure, and has a relatively large specific surface area and prosperous pore structure. It can be seen from Fig. 4(e) and (f) that the SA-BA eutectic mixture uniformly covers the surface of BN. It can be clearly seen from Fig. 4(g) and (h) that the SA-BA eutectic mixture is filled in the pores of EG. Thus, SA-BA eutectic mixture in the liquid phase can be easily filled in this porous structure of EG. Such as Fig. 4(i) and (j) that SA-BA eutectic mixture is absorbed in pores. Obviously, due to the surface tension and the effect of the capillary that the interface between SA-BA eutectic mixture and BN, EG is very compact and there is no obvious phase separation phenomenon.

### 3.3. Chemical compatibility of the SA-BA/BN/EG composite

The FTIR spectra of SA, BN, EG, 15BN, 20EG and 15BN20EG composite are shown in Fig. 5. The typical absorption peaks of SA-BA eutectic mixture are located at 3370.91  $\text{cm}^{-1}$ , 3174.59  $\text{cm}^{-1}$ , 2954.46  $\text{cm}^{-1}$ , 2917.29  $\text{cm}^{-1}$ , 2848.94  $\text{cm}^{-1}$ , 1703.11  $\text{cm}^{-1}$ , 1658.32  $\text{cm}^{-1}$ , 1577.63  $\text{cm}^{-1}$ , 1471.46  $\text{cm}^{-1}$ , 1430.95  $\text{cm}^{-1}$ , 1408.54  $\text{cm}^{-1}$ , 1298.25  $\text{cm}^{-1}$ , 944.40  $\text{cm}^{-1}$ , 791.06  $\text{cm}^{-1}$  and 719.42  $\text{cm}^{-1}$ . The absorption peaks at 3370.91  $\text{cm}^{-1}$  and 3174.59  $\text{cm}^{-1}$  represent the stretching vibration peaks of  $-\text{NH}_2$  in  $\text{C}=\text{O}-\text{NH}_2$ , The absorption peak at 3000–2500  $\text{cm}^{-1}$  is the stretching vibration band of  $-\text{OH}$  in carboxylic acid, the absorption peak at 2954.46  $\text{cm}^{-1}$  represents the asymmetric stretching vibration peak of  $\text{CH}_3$ , the absorption peaks at 2917.29  $\text{cm}^{-1}$  and 2848.94  $\text{cm}^{-1}$  are asymmetric stretching vibration peak and symmetric stretching vibration peak of  $-\text{CH}_2$ , respectively, the absorption peak at 1703.11  $\text{cm}^{-1}$  is attributed to the  $\text{C}=\text{O}$  stretching vibration in

the carboxylic acid, the absorption peak at 1658.32  $\text{cm}^{-1}$  represents the stretching vibration peak of  $\text{C}=\text{O}$  in  $\text{C}=\text{O}-\text{NH}_2$ , the absorption peak at 1577.63  $\text{cm}^{-1}$  is the  $\text{C}-\text{C}$  stretching vibration peak in the benzene ring, the absorption peak at 1471.46  $\text{cm}^{-1}$  is attributed to the asymmetric bending vibration of  $\text{CH}_3$ , the absorption peak at 1430.95  $\text{cm}^{-1}$  is the stretching vibration peak of  $\text{C}-\text{O}$ , the absorption peak at 1408.54  $\text{cm}^{-1}$  is attributed to the bending vibration of  $-\text{CH}_2$ , the absorption peak at 1298.25  $\text{cm}^{-1}$  is attributed to the rocking and twisting vibration of  $-\text{CH}_2$  in long chain fatty acids, respectively, the absorption peak at 944.40  $\text{cm}^{-1}$  is the out of plane deformation vibration peak of  $-\text{OH}$ , the absorption peak at 791.06  $\text{cm}^{-1}$  represents the deformation vibration peak of  $\text{C}-\text{H}$  in the benzene ring, the absorption peak at 719.42  $\text{cm}^{-1}$  is attributed to the in-plane deformation (rocking vibration) of  $-\text{CH}_2$ . In the FTIR spectrum of BN, the main characteristic peaks appear at 1372.66  $\text{cm}^{-1}$  and 816.50  $\text{cm}^{-1}$ , which are assigned to the in-plane stretching vibration and bending vibration of  $\text{B}-\text{N}$  and  $\text{N}-\text{B}-\text{N}$ , respectively. In the FTIR spectrum of EG, the characteristic absorption peaks at 3441.16  $\text{cm}^{-1}$ , 1635.41  $\text{cm}^{-1}$  and 1114.17  $\text{cm}^{-1}$ , which are respectively attributed to the stretching vibration of  $\text{O}-\text{H}$ ,  $\text{C}=\text{O}$  and  $\text{C}-\text{O}$ , indicating that the carbon atoms of graphite are oxidized after strong acid intercalation treatment.

It can be seen from the infrared spectrum of 15BN20EG in the Fig. 5 that its absorption peak is only the sum of the characteristic absorption peaks of SA-BA eutectic mixture, BN and EG, and there is no new absorption peak, these results demonstrate that there is no chemical reaction between them.

### 3.4. Crystallization characteristics of the SA-BA/BN/EG composite

The XRD patterns of SA-BA eutectic mixture, BN, EG, 15BN, 20EG and 15BN20EG, shown in Fig. 6, it reveals that the characteristic peak of BN is located at  $2\theta = 26.74^\circ$  and that of EG is located at  $2\theta = 26.24^\circ$ , and both peaks had high intensity and a sharp shape. The XRD peaks of SA-BA eutectic mixture, are

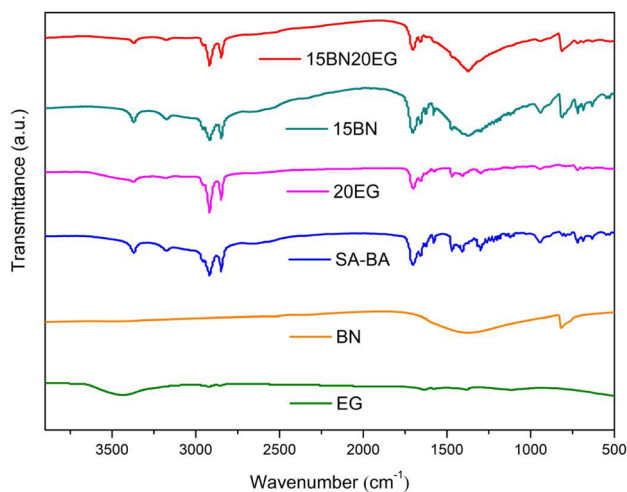


Fig. 5 FTIR spectra of the SA-BA/BN/EG composites.

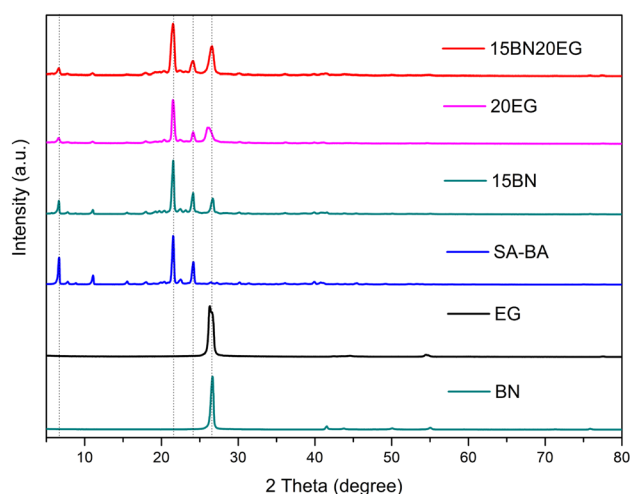


Fig. 6 XRD patterns of SA-BA/BN/EG composite.



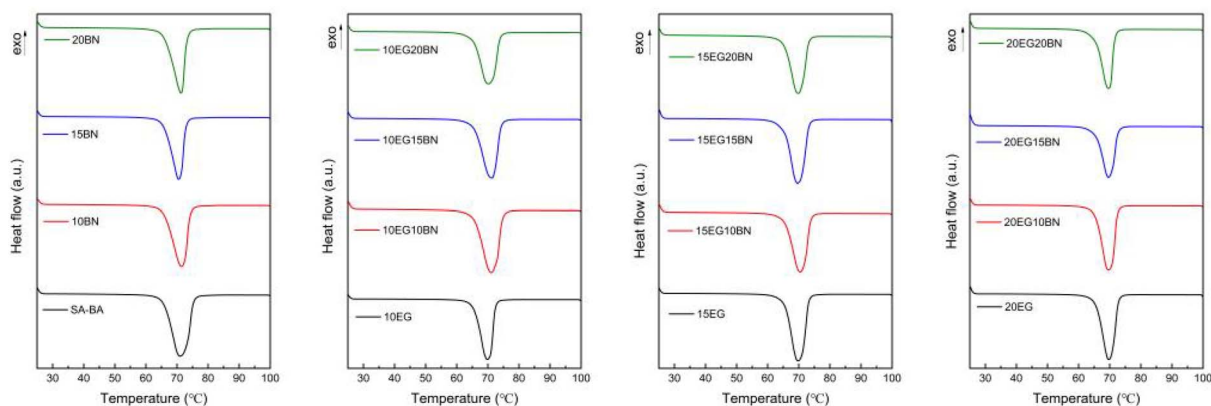


Fig. 7 DSC curves of SA-BA/BN/EG composite during melting processes.

located at  $2\theta = 6.69^\circ$ ,  $21.58^\circ$ , and  $24.23^\circ$ . The above results testify the good crystalline structures of BN, EG and SA-BA eutectic mixture. Besides, the characteristic peaks of BN and SA-BA eutectic mixture can be observed in the peaks of 15BN. the characteristic peaks of EG and SA-BA eutectic mixture can be observed in the peaks of 20EG. Furthermore, the characteristic peaks of 15BN20EG in Fig. 6 also reveal that the addition of BN and EG did not change the positions of the three characteristic peaks of SA-BA eutectic mixture at  $2\theta = 6.59^\circ$ ,  $21.35^\circ$ , and  $24.16^\circ$ . Moreover, the characteristic peaks of EG, BN and SA-BA eutectic mixture, are easily found among the characteristic peaks of 15BN20EG, with only a slight decrease in the absorption intensity, and no new diffraction peaks present. This manifests no chemical interaction among SA-BA eutectic mixture, BN and EG. The composite PCMs prepared by SA-BA eutectic mixture, EG and BN have not changed their respective chemical properties.

### 3.5. Thermal properties of the SA-BA/BN/EG composite

The DSC curves of SA-BA/BN/EG composite with different mass fractions of BN and EG in the melting process are shown in Fig. 7. Additionally, the corresponding thermophysical properties, including melting temperature ( $T_m$ ), melting latent heat ( $\Delta H_m$ ), theoretical enthalpy ( $\Delta H_t$ ), and effective energy per unit mass of SA-BA eutectic mixture ( $E_{ef}$ ) are listed in Table 3. The  $\Delta H_t$  is calculated using the formula (1):

$$\Delta H_t = (1 - \eta)\Delta H_{SA-BA} \quad (1)$$

where,  $\Delta H_t$ ,  $\eta$  and  $\Delta H_{SA-BA}$  are the theoretically calculated phase transition enthalpy of composite, the mass fraction of EG and BN in composite, and the phase transition latent heat of SA-BA eutectic mixture measured by DSC experiment, respectively. Meanwhile  $E_{ef}$ ,  $J g^{-1}$  is given by:

$$E_{ef} = \Delta H_m / (1 - \eta) \quad (2)$$

It can be seen from Fig. 7 that the DSC curves of all materials have only one peak, and the peak position and peak shape are

similar, indicating that the phase change behavior of the prepared composite is mainly generated by SA-BA eutectic mixtures, and no new substances appear. It can be seen from the comparison of DSC curves of SA-BA eutectic mixture and SA-BA/BN/EG composite in Fig. 7, when the EG content is constant, the peak area of the DSC curves gradually decreases with the increase of BN content, which means that the phase change latent heat gradually decreases, indicates that the phase change latent heat of the composite is not provided by BN, but by SA-BA eutectic mixture.

The melting temperature and latent heat of different composites are shown in Table 3. The melting latent heat of SA-BA eutectic mixture is  $202.39 J g^{-1}$ ; When the mass fraction of BN is 15%, the melting latent heat of 15BN composite is  $172.63 J g^{-1}$ , and its melting enthalpy is 85.30% of the SA-BA eutectic mixture; When the mass fraction of BN and EG is 15% and 20% respectively, the melting enthalpy of 15BN20EG composite decreased to  $132.35 J g^{-1}$ , respectively, and its melting enthalpy is 65.39% of that of SA-BA eutectic mixture; it shows that the enthalpy of the composites decreases in direct proportion to the

Table 3 Thermal properties of SA-BA eutectic mixture, SA-BA/BN, SA-BA/EG and SA-BA/BN/EG composite

PCMs	$T_m$ (°C)	$\Delta H_m$ ( $J g^{-1}$ )	$\Delta H_t$ ( $J g^{-1}$ )	$E_{ef}$ ( $J g^{-1}$ )
SA-BA	65.32	202.39	202.39	
10EG	65.31	183.49	182.15	203.88
15EG	65.23	173.93	172.03	204.62
20EG	65.29	165.79	161.91	207.24
10BN	65.40	177.01	182.15	196.68
15BN	65.38	172.63	172.03	203.09
20BN	65.52	160.01	161.91	200.01
10BN10EG	65.37	158.40	161.91	198.00
15BN10EG	65.23	152.54	151.79	203.39
20BN10EG	65.05	143.48	141.67	204.97
10BN15EG	65.26	150.76	151.79	201.01
15BN15EG	65.14	142.33	141.67	203.33
20BN15EG	65.03	131.00	131.55	195.52
10BN20EG	65.16	140.50	141.67	200.71
15BN20EG	65.21	132.35	131.55	203.62
20BN20EG	65.04	120.75	121.43	201.25



amount of BN and EG added. It can be seen from Table 3 that the melting temperature of SA-BA/EG composite is lower than that of SA-BA eutectic mixtures, which decreased by 0.01, 0.09 and 0.03, respectively, it shows that the addition of EG is beneficial to the nucleation of SA-BA eutectic mixtures. Moreover, it can be seen from Table 3 that when the BN content is constant, the melting temperature of the SA-BA/BN/EG composite decreases gradually with the increase of EG content. In addition, when the EG content is constant, the melting temperature of the material decreases gradually with the increase of BN content. The melting and solidification temperature of SA-BA eutectic mixture is 65.32 °C and 64.12 °C respectively; the subcooling is 1.2 °C. When the mass fraction of BN is 15%, the melting and solidification temperature of 15BN composite is 65.38 °C and 63.73 °C respectively, the subcooling is 1.65 °C, which is 0.45 °C higher than that of the SA-BA eutectic mixture. When the mass fraction of BN and EG is 15% and 20% respectively, the melting and solidification temperature of 15BN20EG composite is 65.21 °C and 65.42 °C respectively, the subcooling is 0.21 °C, which is 0.99 °C lower than that of the SA-BA eutectic mixture. These shows that the increase of BN and EG is beneficial to the nucleation of the SA-BA/BN/EG composites. This may be due to the addition of 3D EG and BN structures for the heterogeneous nucleation of SA-BA eutectic mixture in the composite, which act as nucleating agents in the composite.

### 3.6. Thermal conductivity of the SA-BA/BN/EG composite

From the thermal conductivity analysis of SA-BA/BN/EG composite, shown in Fig. 8, indicates that the thermal conductivity of the composite increases with the increase of the EG and BN mass fraction. In particular, the thermal conductivity of composites 10BN, 15BN, 20BN, 10EG, 15EG, 20EG, 10EG10BN, 10EG15BN, 10EG20BN, 15EG10BN, 15EG15BN, 15EG20BN, 20EG10BN, 20EG15BN and 20EG20BN are 0.5878 W m<sup>-1</sup> K<sup>-1</sup>, 0.7278 W m<sup>-1</sup> K<sup>-1</sup>, 0.9647 W m<sup>-1</sup> K<sup>-1</sup>, 3.525 W m<sup>-1</sup> K<sup>-1</sup>, 4.913 W m<sup>-1</sup> K<sup>-1</sup>, 6.377 W m<sup>-1</sup> K<sup>-1</sup>, 3.805 W m<sup>-1</sup> K<sup>-1</sup>,

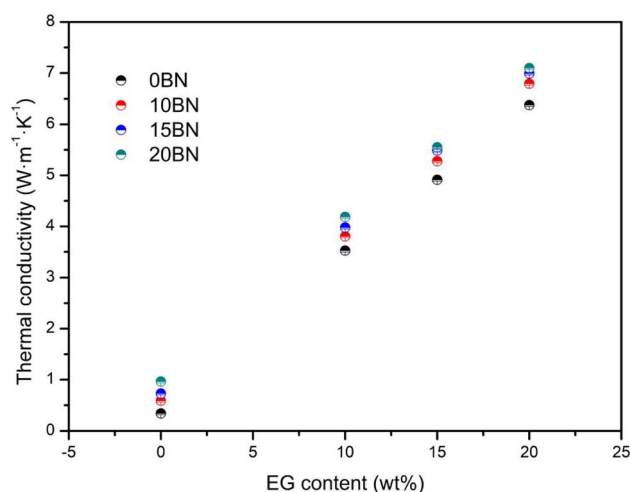


Fig. 8 Thermal conductivity of SA-BA/BN/EG composite.

3.977 W m<sup>-1</sup> K<sup>-1</sup>, 4.184 W m<sup>-1</sup> K<sup>-1</sup>, 5.278 W m<sup>-1</sup> K<sup>-1</sup>, 5.486 W m<sup>-1</sup> K<sup>-1</sup>, 5.552 W m<sup>-1</sup> K<sup>-1</sup>, 6.791 W m<sup>-1</sup> K<sup>-1</sup>, 6.990 W m<sup>-1</sup> K<sup>-1</sup>, 7.097 W m<sup>-1</sup> K<sup>-1</sup>, respectively. Compared with SA-BA eutectic mixture (thermal conductivity is 0.3393 W m<sup>-1</sup> K<sup>-1</sup>), the thermal conductivity increased by 0.732, 1.145, 1.843, 9.389, 13.480, 17.795, 10.214, 10.721, 11.331, 14.556, 15.169, 15.363, 19.015, 19.601, 19.917 time. When the EG content is constant, the thermal conductivity of the composite increased with the increase of the mass fraction of BN. When the mass fraction of EG was 10 wt%, 15 wt% and 20 wt%, respectively, the thermal conductivity of the composite increased by 0.172 and 0.207 W m<sup>-1</sup> K<sup>-1</sup>, 0.208 and 0.066 W m<sup>-1</sup> K<sup>-1</sup>, and 0.199 and 0.107 W m<sup>-1</sup> K<sup>-1</sup>, respectively, for each increase of the mass fraction of BN by 5 wt%. When the mass fraction of BN is constant and the mass fraction of EG is 10%, 15% and 20%, the thermal conductivity of the composite increased by 1.475 and 1.513 W m<sup>-1</sup> K<sup>-1</sup>, 1.509 and 1.504 W m<sup>-1</sup> K<sup>-1</sup>, and 1.368 and 1.545 W m<sup>-1</sup> K<sup>-1</sup>, respectively, for every 5 wt% increase in the mass fraction of EG added. The experimental results show that although BN has excellent thermal conductivity the improvement of the thermal conductivity of SA-BA eutectic mixture is not very obvious, and the improvement of the thermal conductivity is much lower than that of EG at the same mass fraction.

The thermal conductivity of 15BN20EG and those of some of the reported shape stabilized composite PCMs are listed in Table 4. The results show that thermal conductivity of 15BN20EG are comparable or even superior to those previously reported in literature. Therefore, the 15BN20EG is a desirable material for low temperature latent heat storage applications.

### 3.7. Thermal stability analyses of the SA-BA/BN/EG composite

The TGA and DTG curves of SA-BA eutectic mixture, 15BN, 20BN, 20EG, 15BN20EG and 20BN20EG composite from room temperature to 800 °C are shown in Fig. 9, and corresponding data are listed in Table 5. It can be seen from Fig. 9 and Table 5 that the SA-BA eutectic mixture began to decompose at about 161.00 °C and completely decomposed at about 285.30 °C, the initial thermal decomposition temperature of 15BN is 222.30 °C, which is 61.3 °C higher than that of SA-BA eutectic mixture. Besides, it can be seen from the comparison between 15BN and 20BN composite that the thermal decomposition temperature of composite increases with the increase of mass fraction of BN, and in the SA-BA/BN/EG composite, when the mass fraction of EG is constant, the thermal decomposition temperature of the composite increases with the increase of BN mass fraction, which indicates that BN is benefit to improving the thermal stability of SA-BA eutectic mixture. What's more, the SA-BA eutectic mixture is completely decomposed at 285.30 °C, the temperature weight loss did not increase significantly with the increase of temperature in the range of 800 °C. The weight loss trend of the 15BN20EG composite is similar to that of SA-BA eutectic mixture, and the weight loss rate is the largest in the temperature range of 208.20–304.80 °C. The total weight loss of SA-BA eutectic mixture and 15BN20EG is about 100% and



**Table 4** Comparison of thermal properties of SA–BA/BN/EG composite PCMs of this study with previously published studies on similar composite PCMs

Samples	Thermal conductivity ( $\text{W m}^{-1} \text{K}^{-1}$ )	References
SA–BA/15 wt% BN/20 wt% EG	6.990	This work
Epoxy/70 wt% BN/5 wt% EG	2.220	24
SA/12 wt% BN/12 wt% EG	6.349	25
SA/10 wt% ( $\text{Co}_3\text{O}_4$ + EG)	2.530	26
LA/29.8 wt% (Ag–EG)	2.850	27
NaCl–KCl– $\text{MgCl}_2$ /Al/15 wt% EG	5.100	28
1-Octadecanol/10 wt% $\text{Al}_2\text{O}_3$ @EG	1.876	29
Paraffin–HDPE + 4% EG/1% MWCNT	1.360	30
PEG + 4% GO/30% BN	3.000	31
N-Eicosane/ $\text{SiO}_2$ /7 wt% EG	0.334	32
Paraffin/17.5 wt% (graphene oxide/BN)	1.680	33
PEG/27.01 wt% (BN/chitosan)	2.780	34
PEG/30 wt% BN/1 wt% GNP	1.330	35

68.63%, respectively, that's because that the thermal decomposition of 15BN20EG composite is mainly produced by SA–BA eutectic mixture. In addition, the initial weight loss temperature of 15BN, 20EG, and 15BN20EG is increased compared with SA–BA eutectic mixture, which may be due to the presence of capillary and van der Waals forces between SA–BA eutectic mixture and BN, and EG to promote the thermal stability of the composite. In summary, the addition of BN and EG can significantly improve the thermal stability of the composite. The DTG curves also reveal that 15BN20EG hardly decomposes below 208.20 °C, which implies that the working performance of the composite PCMs is relatively stable within the temperature range of 100 °C.

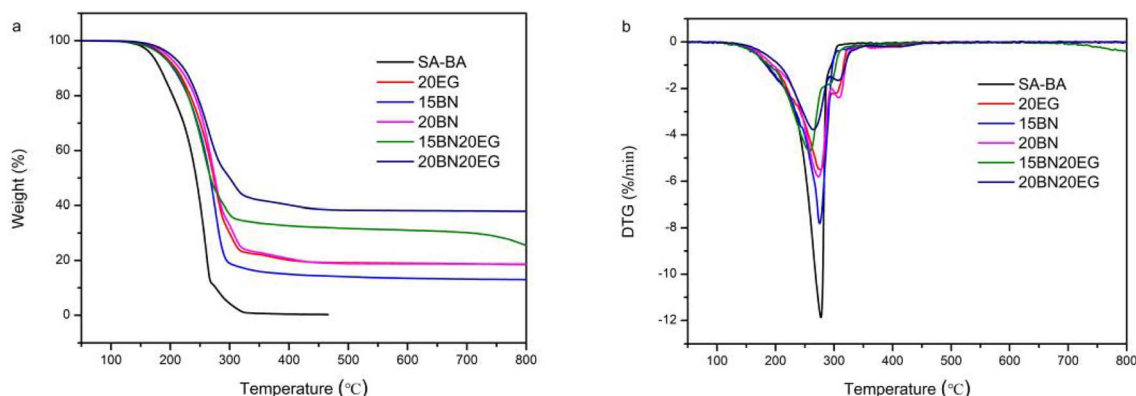
### 3.8. Thermal cycle stability analysis of the SA–BA/BN/EG composite

To determine the feasibility of the application of the 15BN20EG composite, its thermal cycle stability was analyzed by performing 100 DSC heating and cooling cycles. The DSC curves of the 15BN20EG composite at the 1st, 20th, 40th, 60th, 80th, and 100th cycles, shown in Fig. 10, reveal that the peak position of the exothermic curve of 15BN20EG changed with

the increase of number of cycles compared with that at the 1st cycle. Compared with the 1st cycle, the exothermic peak became wide and sharp at the 20 to 100th cycles. Remarkably, the DSC curves also show that the endothermic peak of the composite did not change significantly after multiple cycles. The melting and solidification latent heat in the 1st cycle of the 15BN20EG composite are 126.29 and 123.78  $\text{J g}^{-1}$ ,

**Table 5** Onset decomposition temperature ( $T_{\text{onset}}$ ), Maximum decomposition temperature ( $T_{\text{max}}$ ) end decomposition temperature ( $T_{\text{end}}$ ) and residual weight (RW) for decompositions of SA–BA eutectic mixture, 15BN, 20EG, 10BN20EG, 15BN20EG and 20BN20EG composite

Material	$T_{\text{onset}}$ (°C)	$T_{\text{max}}$ (°C)	$T_{\text{end}}$ (°C)	RW (%)
SA–BA	161.00	277.60	285.30	0.51
15BN	222.30	275.30	292.50	12.85
20BN	225.90	273.30	436.40	18.66
20EG	214.00	277.10	410.60	18.24
10BN20EG	205.40	252.60	311.30	27.69
15BN20EG	208.20	257.70	304.00	31.37
20BN20EG	212.80	264.10	452.60	37.83

**Fig. 9** Curves of (a) TGA and (b) DTG of SA–BA/BN/EG composite.

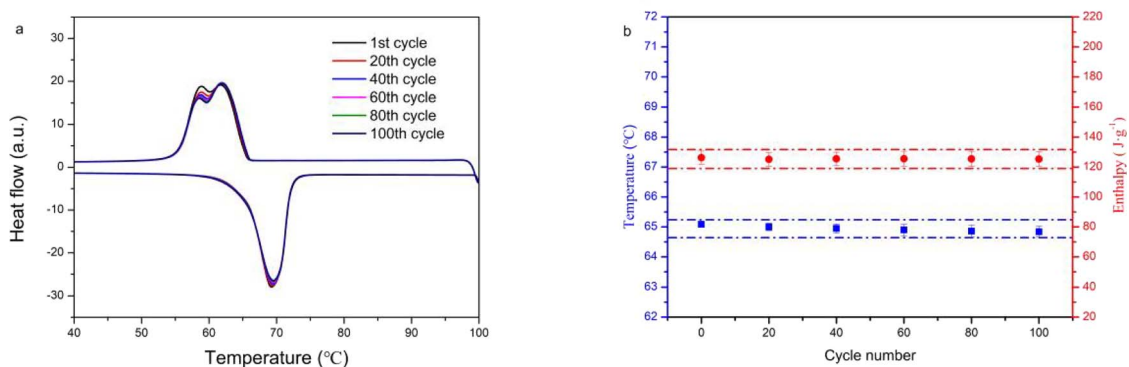


Fig. 10 100 thermal cycle curves of (a) and (b) of 15BN20EG composite.

respectively, and the melting and solidification temperature are 65.09 °C and 65.53 °C, respectively. After 100 DSC heating and cooling cycles, the melting temperature and latent heat of the composite are 64.84 °C and 125.34 J g<sup>-1</sup>, respectively, which are changed 0.45 °C and 0.95 J g<sup>-1</sup>, respectively, than those in the 1st cycle. The solidification temperature and latent heat are 65.88 °C and 123.47 J g<sup>-1</sup>, respectively, which are changed 0.33 °C and 0.31 J g<sup>-1</sup>, respectively, than those in the 1st cycle. In summary, the basic thermo-physical parameters of the composite PCMs did not change significantly after 100 thermal cycles, which indicates that 15BN20EG has excellent cycle stability. Therefore, these materials have good application prospects in the field of low temperature phase transition.

## 4. Conclusions

In this study, ultrasonic and melt adsorption method was used to prepare a new type of high thermal conductive shape-stable SA-BA/BN/EG composite. Eutectic mixture SA-BA was adopted as the phase change material in the composite, EG was used as the inert support matrix to increase its thermal conductivity and provide shape stability, while the dispersion of BN further improved its thermal conductivity. By conducting an analysis of micro-structure, latent heat, melting point, thermal conductivity, thermal stability and thermal cycle, the following conclusions were reached.

(1) SA-BA/BN could be evenly distributed among the EG particles, and the pores and interlayer of EG had good adsorption to SA-BA/BN material. The SA-BA eutectic mixture and EG were highly chemical compatible.

(2) The porous structure of EG could absorb large amount of PCMs and form skeleton structure, which prevents the SA-BA/BN composite from leakage effectively during the melting process.

(3) Adding BN and EG can effectively increase the thermal conductivity of the SA-BA eutectic mixture. By adding 15 wt% BN and 20 wt% EG, the melting latent heat as high as 132.35 J g<sup>-1</sup>, the thermal conductivity increased to 6.990 W m<sup>-1</sup> K<sup>-1</sup> in its solid state, which is 20.601 times higher than that of SA-BA eutectic mixture.

(4) After 100 thermal cycles, the melting point, latent heat of the 15BN20EG composite has barely change, which certify that the composite has good thermal stability. Besides, 15BN20EG composite did not decompose below 100 °C, which indicates that 15BN20EG composite has good thermal stability.

## Abbreviations

$T_m$	Melting temperature, °C
$\Delta H_m$	Melting latent heat, J g <sup>-1</sup>
$\Delta H_t$	Theoretical enthalpy, J g <sup>-1</sup>
$E_{ef}$	Effective energy per unit mass, J g <sup>-1</sup>
$\eta$	Mass fraction
$\Delta H_{SA-BA}$	The phase transition latent heat of SA-BA eutectic mixture measured by DSC experiment, J g <sup>-1</sup>
$T_{onset}$	Onset decomposition temperature
$T_{max}$	Maximum decomposition temperature
$T_{end}$	End decomposition temperature
RW	Residual weight
SA	Stearic acid
BA	Benzamide
SA-BA	Stearic acid-benzamide eutectic mixture
BN	Boron nitride
PCMs	Phase change materials

## Conflicts of interest

We declare that we do not have any commercial or associative interest that represents a conflict of interest in connection with the work submitted.

## Acknowledgements

This study was supported by Engineering Research Center of Nuclear Technology Application (East China University of Technology), Ministry of Education (HJSJYB2022-6), Research Foundation for Advanced Talents of East China University of Technology (DHBK2019091), Research Foundation for Advanced Talents of East China University of Technology (No. DHBK2019132).



## References

- 1 Y. Yuan, N. Zhang, W. Tao, *et al.*, Fatty acids as phase change materials: a review, *Renewable Sustainable Energy Rev.*, 2014, **29**, 482–498.
- 2 K. Kant, A. Shukla and A. Sharma, Ternary mixture of fatty acids as phase change materials for thermal energy storage applications, *Energy Rep.*, 2016, **2**, 274–279.
- 3 S. S. Magendran, F. S. A. Khan, N. M. Mubarak, *et al.*, Synthesis of organic phase change materials (PCMs) for energy storage applications: a review, *Nano-Struct. Nano-Objects*, 2019, **20**, 100399.
- 4 I. Baskar, M. Chellapandian and K. Jeyasubramanian, LA–PA eutectic/nano-SiO<sub>2</sub> composite phase change material for thermal energy storage application in buildings, *Constr. Build. Mater.*, 2022, **338**, 127663.
- 5 Z. Luo, H. Zhang, X. Gao, *et al.*, Fabrication and characterization of form-stable capric–palmitic–stearic acid ternary eutectic mixture/nano-SiO<sub>2</sub> composite phase change material, *Energy Build.*, 2017, **147**, 41–46.
- 6 D. Su, Y. Jia, G. Alva, *et al.*, Preparation and thermal properties of n-octadecane/stearic acid eutectic mixtures with hexagonal boron nitride as phase change materials for thermal energy storage, *Energy Build.*, 2016, **131**, 35–41.
- 7 X. Zhang, D. Pan and G. Zhu, Preparation and characterization of form-stable phase-change materials with enhanced thermal conductivity based on nano-Al<sub>2</sub>O<sub>3</sub> modified binary fatty acids and expanded perlite, *Energy Build.*, 2022, **271**, 112330.
- 8 X. Qiao, X. Kong and L. Wang, Thermal performance analysis of a thermal enhanced form-stable composite phase change material with aluminum nitride, *Appl. Therm. Eng.*, 2021, **187**, 116581.
- 9 L. Yang, N. Zhang, Y. Yuan, *et al.*, Thermal performance of stearic acid/carbon nanotube composite phase change materials for energy storage prepared by ball milling, *Int. J. Energy Res.*, 2019, **43**(12), 6327–6336.
- 10 R. Zhang, D. Chen, L. Chen, *et al.*, Preparation and thermal properties analysis of fatty acids/1-hexadecanol binary eutectic phase change materials reinforced with TiO<sub>2</sub> particles, *J. Energy Storage*, 2022, **51**, 104546.
- 11 G. R. Bhimanapati, N. R. Glavin and J. A. Robinson, *2D Boron Nitride: Synthesis and Applications//Semiconduc. Semimet.*, Elsevier, 2016, 95, pp. 101–147.
- 12 L. Lindsay and D. A. Broido, Enhanced thermal conductivity and isotope effect in single-layer hexagonal boron nitride, *Phys. Rev. B: Condens. Matter Mater. Phys.*, 2011, **84**(15), 155421.
- 13 H. Shen, J. Guo, H. Wang, *et al.*, Bioinspired modification of h-BN for high thermal conductive composite films with aligned structure, *ACS Appl. Mater. Interfaces*, 2015, **7**(10), 5701–5708.
- 14 H. Shen, C. Cai, J. Guo, *et al.*, Fabrication of oriented hBN scaffolds for thermal interface materials, *RSC Adv.*, 2016, **6**(20), 16489–16494.
- 15 Z. Lin, Y. Liu, S. Raghavan, *et al.*, Magnetic alignment of hexagonal boron nitride platelets in polymer matrix: toward high performance anisotropic polymer composites for electronic encapsulation, *ACS Appl. Mater. Interfaces*, 2013, **5**(15), 7633–7640.
- 16 X. Fang, L. W. Fan, Q. Ding, *et al.*, Thermal energy storage performance of paraffin-based composite phase change materials filled with hexagonal boron nitride nanosheets, *Energy Convers. Manage.*, 2014, **80**, 103–109.
- 17 Y. Xiao, W. Wang, T. Lin, *et al.*, Largely enhanced thermal conductivity and high dielectric constant of poly(vinylidene fluoride)/boron nitride composites achieved by adding a few carbon nanotubes, *J. Phys. Chem. C*, 2016, **120**(12), 6344–6355.
- 18 B. Xie, C. Li, J. Chen, *et al.*, Exfoliated 2D hexagonal boron nitride nanosheet stabilized stearic acid as composite phase change materials for thermal energy storage, *Sol. Energy*, 2020, **204**, 624–634.
- 19 C. Ao, S. Yan, X. Zhao, *et al.*, Stearic acid/boron nitride as a composite phase change material for thermal energy storage, *Diamond Relat. Mater.*, 2023, 109671.
- 20 D. Su, Y. Jia, G. Alva, *et al.*, Preparation and thermal properties of n-octadecane/stearic acid eutectic mixtures with hexagonal boron nitride as phase change materials for thermal energy storage, *Energy Build.*, 2016, **131**, 35–41.
- 21 Z. Wang, G. Huang, Z. Jia, *et al.*, Eutectic Fatty Acids Phase Change Materials Improved with Expanded Graphite, *Materials*, 2022, **15**(19), 6856.
- 22 D. Zhou, J. Yuan, Y. Zhou, *et al.*, Preparation and characterization of myristic acid/expanded graphite composite phase change materials for thermal energy storage, *Sci. Rep.*, 2020, **10**(1), 10889.
- 23 G. Ma, J. Sun, Y. Zhang, *et al.*, Preparation and thermal properties of stearic acid–benzamide eutectic mixture/expanded graphite composites as phase change materials for thermal energy storage, *Powder Technol.*, 2019, **342**, 131–140.
- 24 I. Isarn, L. Bonnaud, L. Massagues, *et al.*, Enhancement of thermal conductivity in epoxy coatings through the combined addition of expanded graphite and boron nitride fillers, *Prog. Org. Coat.*, 2019, **133**, 299–308.
- 25 C. Ao, S. Yan, L. Zhao, *et al.*, Design of a stearic acid/boron nitride/expanded graphite multifiller synergistic composite phase change material for thermal energy storage, *Energy Built Environ.*, 2022, DOI: [10.1016/j.enbenv.2022.04.004](https://doi.org/10.1016/j.enbenv.2022.04.004).
- 26 D. Li, X. Cheng, Y. Li, *et al.*, Effect of MOF derived hierarchical Co<sub>3</sub>O<sub>4</sub>/expanded graphite on thermal performance of stearic acid phase change material, *Sol. Energy*, 2018, **171**, 142–149.
- 27 R. Wen, S. Zhu, M. Wu, *et al.*, Design and preparation of Ag modified expanded graphite based composite phase change materials with enhanced thermal conductivity and light-to-thermal properties, *J. Energy Storage*, 2021, **41**, 102936.
- 28 X. Ran, H. Wang, Y. Zhong, *et al.*, Thermal properties of eutectic salts/ceramics/expanded graphite composite phase change materials for high-temperature thermal energy storage, *Sol. Energy Mater. Sol. Cells*, 2021, **225**, 111047.



- 29 S. Gong, X. Cheng, Y. Li, *et al.*, Enhancement of ceramic foam modified hierarchical  $\text{Al}_2\text{O}_3$ @ expanded graphite on thermal properties of 1-octadecanol phase change materials, *J. Energy Storage*, 2019, **26**, 101025.
- 30 Y. Qu, S. Wang, D. Zhou, *et al.*, Experimental study on thermal conductivity of paraffin-based shape-stabilized phase change material with hybrid carbon nano-additives, *Renewable Energy*, 2020, **146**, 2637–2645.
- 31 J. Yang, L. S. Tang and R. Y. Bao, Hybrid network structure of boron nitride and graphene oxide in shape-stabilized composite phase change materials with enhanced thermal conductivity and light-to-electric energy conversion capability, *Sol. Energy Mater. Sol. Cells*, 2018, **174**, 56–64.
- 32 X. Zhang, C. Zhu and G. Fang, Preparation and thermal properties of n-eicosane/nano- $\text{SiO}_2$ /expanded graphite composite phase-change material for thermal energy storage, *Mater. Chem. Phys.*, 2020, **240**, 122178.
- 33 J. Yang, L. S. Tang, R. Y. Bao, *et al.*, Hybrid network structure of boron nitride and graphene oxide in shape-stabilized composite phase change materials with enhanced thermal conductivity and light-to-electric energy conversion capability, *Sol. Energy Mater. Sol. Cells*, 2018, **174**, 56–64.
- 34 X. Jia, Q. Li, C. Ao, *et al.*, High thermal conductive shape-stabilized phase change materials of polyethylene glycol/boron nitride@ chitosan composites for thermal energy storage, *Composites, Part A*, 2020, **129**, 105710.
- 35 J. Yang, L. S. Tang, R. Y. Bao, *et al.*, Largely enhanced thermal conductivity of poly (ethylene glycol)/boron nitride composite phase change materials for solar-thermal-electric energy conversion and storage with very low content of graphene nanoplatelets, *Chem. Eng. J.*, 2017, **315**, 481–490.

